



Performance of $\text{La}_{0.1}\text{Sr}_{0.9}\text{Co}_{0.8}\text{Fe}_{0.2}\text{O}_{3-\delta}$ and $\text{La}_{0.1}\text{Sr}_{0.9}\text{Co}_{0.8}\text{Fe}_{0.2}\text{O}_{3-\delta}-\text{Ce}_{0.9}\text{Gd}_{0.1}\text{O}_2$ oxygen electrodes with $\text{Ce}_{0.9}\text{Gd}_{0.1}\text{O}_2$ barrier layer in reversible solid oxide fuel cells

Moon-Bong Choi ^a, Bhupendra Singh ^{a,b}, Eric D. Wachsman ^c, Sun-Ju Song ^{a,b,*}

^a Ionics Lab, School of Materials Science and Engineering, Chonnam National University, 300 Yongbong-dong, Buk-gu, Gwang-Ju 500-757, Republic of Korea

^b Research Institute for Catalysis, Chonnam National University, 300 Yongbong-dong, Buk-gu, Gwang-Ju 500-757, Republic of Korea

^c Department of Materials Science and Engineering, University of Maryland, College Park, MD 20742, USA



HIGHLIGHTS

- Button cells with LSCF1982-based oxygen electrodes are tested for RSOCs.
- GDC barrier layer prevents reaction between LSCF1982 and YSZ.
- Button cells show stable galvanostatic SOEC operation for 72 h.
- Reversibility is tested by successive SOFC → SOEC → SOFC operations.
- Possible reasons of irreversibility are discussed.

ARTICLE INFO

Article history:

Received 23 January 2013

Received in revised form

15 March 2013

Accepted 19 March 2013

Available online 5 April 2013

Keywords:

Reversible solid oxide cell

Solid oxide electrolysis cell

Tape casting

Barrier layer

ABSTRACT

$\text{La}_{0.1}\text{Sr}_{0.9}\text{Co}_{0.8}\text{Fe}_{0.2}\text{O}_{3-\delta}$ (LSCF1982) and $\text{La}_{0.1}\text{Sr}_{0.9}\text{Co}_{0.8}\text{Fe}_{0.2}\text{O}_{3-\delta}-\text{Ce}_{0.9}\text{Gd}_{0.1}\text{O}_2$ (LSCF1982–GDC) composite oxygen electrodes with a GDC barrier layer are tested in yttria stabilized zirconia (YSZ) electrolyte-based reversible solid oxide cells (RSOCs). Three button cell assemblies (1: $\text{NiO}-\text{YSZ}|\text{YSZ}/\text{GDC}|\text{LSCF1982}$; 2: $\text{NiO}-\text{YSZ}/\text{NiO}-\text{YSZ}|\text{YSZ}/\text{GDC}|\text{LSCF1982}$; and 3: $\text{NiO}-\text{YSZ}/\text{NiO}-\text{YSZ}|\text{YSZ}/\text{GDC}|\text{LSCF1982}-\text{GDC}$) are fabricated and their performance in solid oxide fuel cell (SOFC) and solid oxide electrolysis cell (SOEC) modes are studied at different temperatures ($600 \leq T/\text{°C} \leq 800$). The use of porous $\text{NiO}-\text{YSZ}$ functional layer between hydrogen electrode and electrolyte leads to improvements in SOFC and SOEC (SOFC/SOEC) performance by improving the diffusion of reacting species inside the electrode. The effect of nature of oxygen electrode on SOFC/SOEC performance is studied, which indicates LSCF1982 oxygen electrode gives better performance than LSCF1982–GDC composite oxygen electrode, but LSCF1982–GDC composite oxygen electrode is more durable during reversible SOFC/SOEC operations. Stability of the button cells is studied in galvanostatic SOEC operation for 72 h and in reversible SOFC/SOEC operations. Current–voltage ($I-V$) tests and Electrochemical Impedance Spectroscopy (EIS) measurements indicate that the button cells show stable operation in SOEC mode. But successive SOFC → SOEC → SOFC operations indicate that the cells are not completely reversible. The possible reason for poor reversibility is found to be related with the grain growth in LSCF1982-based oxygen electrodes.

© 2013 Elsevier B.V. All rights reserved.

1. Introduction

Reversible solid oxide cells capable of working as SOFC for electricity generation from fuel and as SOEC for fuel generation

form electrolysis of steam and CO_2 have created increased interest in the field of development of environmentally friendly ways of energy storage and electricity generation [1,2]. A RSOC system has the potential to be used as an efficient electrical energy storage device at the power plants based on intermittent renewable energy sources and could provide effective and flexible power delivery, and its smaller modules, acting as a rechargeable battery, could play an important role in distributed power generation [3,4]. Also, the possibility of utilization of waste heat generated by high temperature industrial

* Corresponding author. School of Materials Science and Engineering, Chonnam National University, 300 Yongbong-dong, Buk-gu, Gwang-Ju 500-757, Republic of Korea. Tel.: +82 62 530 1706; fax: +82 62 530 1699.

E-mail address: song@chonnam.ac.kr (S.-J. Song).

processes and excess electricity produced in off-peak hours at conventional power plants and renewable sources for steam electrolysis in SOEC has made this technology more attractive [5–7].

Although in principle SOEC is a reverse mode of SOFC as schematically represented in Fig. 1, individual modes presents somewhat different conditions at the electrodes during its operation. Therefore, the selection of suitable electrolyte and electrode materials compatible for stable operation in SOFC mode as well as in SOEC mode is important factor for designing a RSOC. YSZ and Ni–YSZ, respectively, have been widely used electrolyte and hydrogen electrode for SOEC and SOEC [6,8]. Though the composite of lanthanum strontium manganite with YSZ (LSM–YSZ) is widely used as oxygen electrode in SOEC, composites of other perovskite materials, such as lanthanum strontium ferrite (LSF), lanthanum strontium copper ferrite (LSCuF), lanthanum strontium cobalt ferrite (LSCoF), and lanthanum strontium cobaltite (LSCo), with YSZ can be potential material for oxygen electrode [1,9–13]. Since the energy losses due to electrode polarization, especially that of oxygen electrode, and degradation due to the delamination of oxygen electrode, have often been limiting factors in deciding the performance and practicability of SOECs, considerable efforts have been made to improve the performance of oxide electrode [6,14]. Because of their high catalytic activity and oxygen permeability, Co-based perovskite materials could be potential oxygen electrode in SOEC, but during the operation at high temperature they suffer from the drawback of reaction with YSZ electrolyte [15]. By applying a thin layer of another electrolyte, which does not reacts with YSZ at high temperature and, therefore, acts as a barrier layer to prevent the interfacial reaction between YSZ electrolyte and Co-based perovskite oxygen electrode, this drawback could be avoided [16].

In previous works, we have investigated electrochemical properties of LSCF1982 [17–20]. We have employed microwave heat-treated LSCF1982 as a cathode for ceria electrolyte-based intermediate temperature fuel cell and found that, at 650 °C, the fuel cell with microwave heat-treated cathode shows better performance than conventional heat treated cathode [20]. Based on our previous findings in ref. 20, it would be interesting to analyze the performance of LSCF1982 as oxygen electrode in RSOC at the temperatures $600 \leq T/\text{°C} \leq 800$. But, like other Co-based perovskite materials, LSCF1982 suffers from the drawback of interfacial reaction between LSCF1982-based electrodes and YSZ electrolyte. Doped ceria-based materials show no reactivity with LSCF1982 and they can be used as electrolyte with LSCF1982-based

electrodes, but their narrow electrolytic regime, because of partial reduction of Ce^{4+} to Ce^{3+} under reducing conditions, makes them less favorable [16,21,22]. Notwithstanding the above fact, doped ceria, such as GDC, can be used as a barrier layer to avoid interfacial reaction between LSCF1982-based oxygen electrode and YSZ electrolyte.

The optimization of electrode configuration and microstructure has been found to be quite beneficial for the performance of SOFCs, suggesting that such manipulations could be important factor for the RSOCs' performance as well [23]. The introduction of an electrode functional layer between an electrode and an electrolyte has shown to be effective for the improvement of cell performance. Similarly, the use of composite electrodes, having electrolyte as one of its constituents, help improving the stability of cell by enhancing the compatibility of electrolyte and electrode materials at their interface. In previous studies on single RSOCs, SOFC and SOEC modes have shown differences in performance, primarily because of differential behavior of cell components during SOFC/SOEC modes [1,12,13,24,25]. Ni–YSZ fuel electrodes were found to be less active in SOEC mode than in SOFC mode due to the contribution of a diffusion-limited process during SOEC operation [24], and Ni–YSZ fuel electrodes were reported to be susceptible to aging in high-steam environment, because of coarsening of Ni particles [25]. O'Brien et al. [12] have demonstrated that a single cell with Ni–YSZ fuel electrode and LSM oxygen electrode showed small difference in the values of area specific resistance (ASR) in SOFC and SOEC modes. But a study by Eguchi et al. [13] showed a strong dependence of electrode polarization on the operation condition of SOFC and SOEC, and a cell with Ni–YSZ hydrogen electrode and LSM oxygen electrode resulted in small electrode polarization during SOFC operation whereas a cell with Pt hydrogen electrode and LSCo oxygen electrode showed small electrode polarization in SOEC condition. Also, they studied the reversibility of SOFC and SOEC as a function of the H_2O partial pressure ($p_{\text{H}_2\text{O}}$) and H_2 partial pressure (p_{H_2}) in the $\text{H}_2\text{–H}_2\text{O}$ mixture and observed significant concentration overvoltage in the $I\text{–V}$ characteristics of SOFC and SOEC operating in different $p_{\text{H}_2\text{O}}$ and p_{H_2} atmospheres. Marina et al. [1] compared the inefficiencies associated with electrode reactions during SOFC and SOEC operations using RSOCs with Ni–YSZ or $\text{La}_{0.35}\text{Sr}_{0.65}\text{TiO}_3\text{–Ce}_{0.5}\text{La}_{0.5}\text{O}_{2-\delta}$ composite as hydrogen electrode and LSF, LSCuF, LSCoF or LSM as oxygen electrode.

Therefore, considering the above mentioned factors to improve solid oxide cell performance, in the present work, we design three different single cell configurations, primarily based on YSZ electrolyte with a GDC barrier layer, Ni–YSZ hydrogen electrode and LSCF1982 or LSCF1982–GDC composite oxygen electrode, as given below:

Button cell 1 $\text{NiO–YSZ|YSZ|GDC|LSCF1982}$

Button cell 2 $\text{NiO–YSZ|NiO–YSZ|YSZ|GDC|LSCF1982}$

Button cell 3 $\text{NiO–YSZ|NiO–YSZ|YSZ|GDC|LSCF1982–GDC}$

GDC layer is employed as a barrier to prevent the reaction between YSZ and LSCF1982 at the electrolyte/oxygen electrode interface. The introduction of a porous NiO–YSZ functional layer between the dense electrolyte and the hydrogen electrode substrate is to improve the diffusion of reactants inside the electrode. The comparative performances of these single cells as intermediate temperature RSOCs in SOFC mode and SOEC mode are analyzed with respect to variations in oxygen electrode composition, and hydrogen electrode configuration. $I\text{–V}$ measurements and EIS are used for the electrochemical characterization of the cells. We investigate the performance stability of cells 2 and 3 during galvanostatic SOEC operation for 72 h. Also, the reversibility of the button cells is tested by successive SOFC → SOEC → SOFC operations.

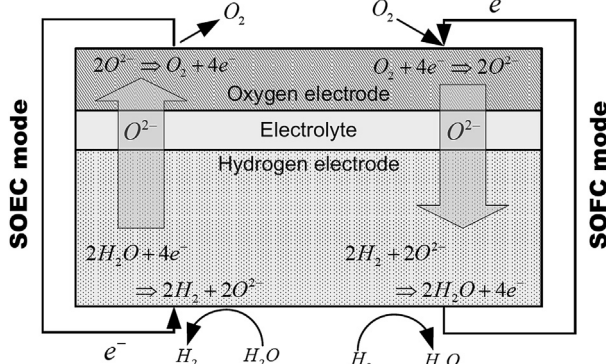


Fig. 1. Schematic representation of processes occurring in a RSOC during the operation in SOFC and SOEC modes.

2. Experimental

2.1. Button cell fabrication

Table 1 shows the details of various steps involved in button cell fabrication. NiO–YSZ hydrogen electrode was prepared by tape casting method [20]. A slurry of NiO (Kceracell; BET = 4–6 m² g⁻¹) and YSZ (Tosoh Advanced Ceramics, TZ-8Y; BET = 13–19 m² g⁻¹) was prepared in two steps. Firstly, NiO and YSZ powders were dispersed with fish oil (Aldrich) as a dispersant in a binary solvent (toluene:ethanol = 1:1 wt%) system for 24 h by ball-mill. Then, butyl benzyl phthalate (BBP) and polyethylene glycol (PEG) were added as plasticizer and polyvinyl butyral 79 (PVB79) was added as binder, and the mixture was ball-milled for 24 h. A de-airing process was conducted to prevent the possible defects caused by air bubbles present in the slurry. NiO–YSZ hydrogen electrode tapes were fabricated by a tape casting process, and 25 mm diameter circles were punched from the obtained green sheet (~350 μm thick). Finally, the circular tapes were partially sintered at 900 °C for 2 h to get as-prepared NiO–YSZ hydrogen electrode.

For button cell 2 and 3, a NiO–YSZ functional layer was applied to as-prep NiO–YSZ hydrogen electrode by dip coating method. The functional layer coating slurry of NiO (Kceracell; BET = 8–12 m² g⁻¹)–YSZ (Tosoh Advanced Ceramics, TZ-8Y; BET = 13–19 m² g⁻¹) was prepared in an ethanol based solvent [26], and functional layer coated samples were heat-treated at 400 °C for 2 h to burn out the organic materials present in the coating slurry and to get as-prepared NiO–YSZ/NiO–YSZ assembly.

YSZ electrolyte was coated over the non-coated (NiO–YSZ) and functional layer-coated (NiO–YSZ/NiO–YSZ) hydrogen electrode samples by dip coating method. The electrolyte coating slurry of YSZ (Tosoh Advanced Ceramics, TZ-8Y; BET = 13–19 m² g⁻¹) was prepared in an ethanol based solvent [26]. The electrolyte coated samples were sintered at 1400 °C for 5 h in air atmosphere. The linear shrinkage rate on sintering was about 20%. Then, GDC barrier layer was coated onto the YSZ electrolyte surface by dip coated method with a coating slurry prepared with 5 g GDC (Kceracell), 40 g ethanol, 0.5 g Solsperse, 0.1 g PEG and 0.2 g PVB79 following the method earlier used for functional layer coating slurry [26], and then heat-treated in microwave oven at 1400 °C for 5 min, which led to the formation of as-prepared (NiO–YSZ|YSZ/GDC) and (NiO–YSZ/NiO–YSZ |YSZ/GDC) assemblies.

Table 1
Details of various steps involved in button cell fabrication.

Button cell fabrication step ^a	Details
<i>Hydrogen electrode</i>	
1. NiO–YSZ substrate ^b	(1) NiO–YSZ tape casting (Thickness = 300 μm) (2) Partial sintering (900 °C, 2 h)
2. NiO–YSZ functional layer ^b	(1) Dip-coating method (Thickness = 15–20 μm) (2) Heat treatment (400 °C, 1 h)
<i>Electrolyte</i>	
3. YSZ electrolyte	(1) Dip-coating method (Thickness = 6–10 μm) (2) Sintering (1400 °C, 5 h)
4. GDC barrier layer	(1) Dip-coating method (Thickness = 1–2 μm) (2) Microwave-assisted heat treatment (1400 °C, 5 min)
<i>Oxygen electrode</i>	
5. LSCF1982	(1) Screen printing (Thickness = 20–25 μm) (2) Microwave-assisted heat treatment (950 °C, 2 min)
6. LSCF1982–GDC ^c	(1) Screen printing (Thickness = 20–25 μm) (2) Microwave-assisted heat treatment (1000 °C, 2 min)

^a Steps for Button cell 1: 1 → 3 → 4 → 5; Button cell 2: 1 → 2 → 3 → 4 → 5; Button cell 3: 1 → 2 → 3 → 4 → 6.

^b Weight ratio of NiO and YSZ in substrate and functional layer; NiO:YSZ = 6:4.

^c Weight ratio of LSCF1982 and GDC in LSCF1982–GDC; LSCF1982:GDC = 50:50.

LSCF1982 powder was synthesized by solid state reaction method [20]. Briefly, La₂O₃ (Alfa Aesar, 99.9%), SrCO₃ (Alfa Aesar, 99.9%), Co₃O₄ (Alfa Aesar, 99.9%), and Fe₂O₃ (Alfa Aesar, 99.99%) were mixed in stoichiometric amounts and the mixture was ball-milled for 24 h with ethanol solvent and calcined at 1000 °C for 12 h in air to get crystalline LSCF1982. The calcined powder was then planetary ball-milled with stabilized zirconia balls for 4 h at 320 rpm. 50 wt. % GDC was used for preparation of LSCF1982–GDC composite. LSCF1982 and LSCF1982–GDC composite paste were prepared using a planetary centrifugal mixer (Thinky, AR-100) with vehicle (ESL, type-441). The pastes were coated over the GDC side of the as-prepared (NiO–YSZ|YSZ/GDC) and (NiO–YSZ/NiO–YSZ|YSZ/GDC) assemblies by screen printing method to complete the button cell assemblies. Finally, the button cells were heat-treated in microwave furnace for 2 min (at 950 °C for button cells 1 and 2 with LSCF1982; and at 1000 °C for button cell 3 with LSCF1982–GDC composite). The area of the oxygen electrode layer over the GDC barrier layer was ~0.5 cm².

2.2. Cell measurement

The schematic representation of experimental setup of RSOC measurement system is shown in Fig. 2. The button cell performance of SOFC and SOEC were evaluated at different temperatures (600 ≤ T/°C ≤ 800) using a lab-made test system. The hydrogen electrode side was sealed with a high temperature ceramic adhesive (Aremco Ceramabond™ 571). Silver meshes were used as current collector for both the hydrogen and oxygen electrodes. Two Pt wires connected to the each sides of silver mesh were used as voltage and current probes, respectively.

Current–voltage measurements and EIS measurements were carried out using a potentiostat (Reference 3000, Gamry Instruments). The frequency range for the EIS measurement was 1–100 kHz. During the SOFC performance test, air and wet hydrogen (3% H₂O) were supplied respectively to the oxygen electrode and hydrogen electrode at a flow rate of 100 standard cubic centimeters (sccm), unless mentioned otherwise. On the other hand, for SOEC test, air (100 sccm) was supplied to the oxygen electrode, and a 50 sccm hydrogen gas and 7 ml h⁻¹ water mixture was supplied to the hydrogen electrode. The flow rate of gases was controlled by mass flow meter while the flow of water was controlled by a syringe pump.

3. Results and discussion

3.1. Material characterization

Fig. 3 shows XRD pattern of LSCF1982 powder calcined at 1000 °C in air for 12 h. The presence of sharp peaks reflects a well-

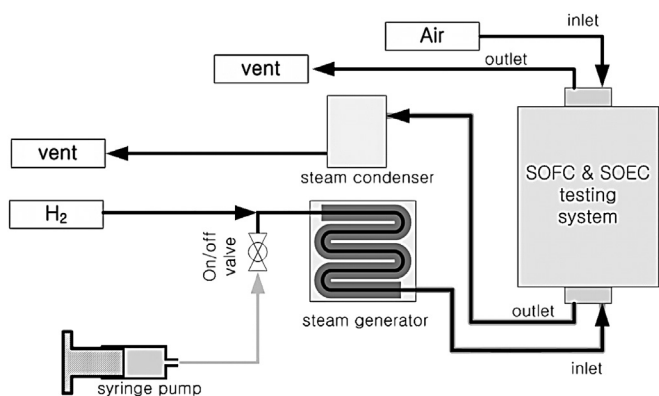


Fig. 2. Schematic representation of experimental setup of RSOC measurement system.

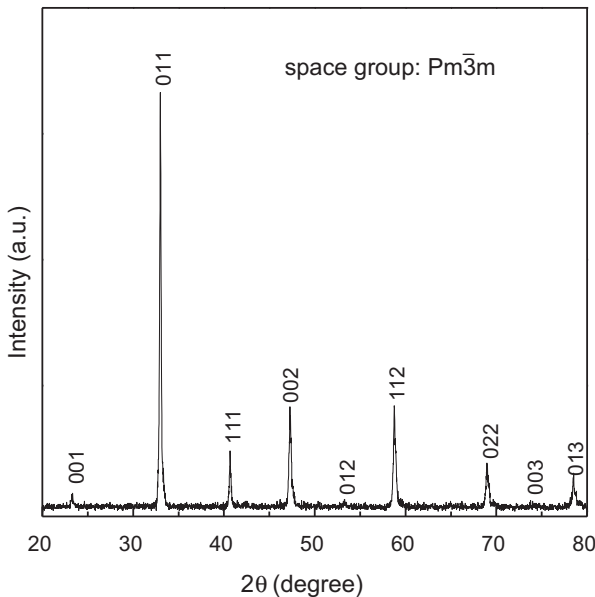


Fig. 3. XRD of LSCF1982 powder calcined at 1000 °C in air for 12 h.

developed crystallized phase and all peaks can be indexed to a cubic perovskite structure with space group $Pm\bar{3}m$, indicating that the single crystalline phase of LSCF1982 is successfully obtained after calcination.

3.2. SOFC operation of button cells

3.2.1. SOFC operation of button cell 1

Firstly, the performance of various button cells was evaluated in SOFC mode. Fig. 4(a) shows $I-V$ test of button cell 1 at different temperatures. The open circuit voltage (OCV) of the cell is nearly constant at 1.05 V at temperatures from 600 to 750 °C. The cell voltage, however, decreases rapidly with the increasing current density at temperatures ≤ 650 °C due to slow electrode kinetics leading to high polarization loss at the lower temperatures. When temperature is increased to 700 and 750 °C, there is significant improvement in electrode kinetics, leading to reduction in electrode polarization loss at these temperatures. The maximum power density (MPD) at 600 and 650 °C is 0.18 and 0.38 $W\text{cm}^{-2}$, respectively and it further increases to 0.74 and 1.54 $W\text{cm}^{-2}$ with increasing temperature to 700 and 750 °C, respectively. The

improvement in MPD with the increase in temperature is due to the reduction in ASR of the cell, as calculated from the EIS spectra shown in Fig. 4(b). The impedance spectrum consists of an elongated arc with a high frequency intercept on the real axis. The high frequency intercept is due to ohmic resistance, mainly ascribed to the electrolyte, whereas the elongated arc corresponds to the electrode phenomena. The appearance of an elongated arc indicates that more than one limiting phenomena are contributing to the processes at the electrode. The contributions of electrode ASR and ohmic ASR is calculated by fitting EIS data with an equivalent circuit shown in Fig. 4(c), where L is the inductance and R is ohmic resistance; resistance $R1$ and constant phase element CPE1 correspond to the charge transfer reaction at the electrode/electrolyte interface, and resistance $R2$ and constant phase element CPE2 correspond to the adsorption/desorption and diffusion inside the porous electrode [27].

The ASR values calculated from the equivalent circuit fitting are given in Table 2, and it is evident that the electrode ASR is the major contributing factor in the total ASR. The increase in temperature makes significant improvement in electrode kinetics and consequently reduces the loss due to the electrode polarization, and therefore, the values of electrode ASR decrease significantly with the increasing temperature and leads to improvements in cell voltage and power density, as shown in Fig. 4(a).

3.2.2. SOFC operation of button cell 2

The button cell 2 consists of an additional functional layer of porous NiO–YSZ between YSZ electrolyte and NiO–YSZ hydrogen electrode. Fig. 5(a) shows the SOFC performance of button cell 2 at different temperatures. At 650 °C, OCV and MPD are 1.12 V and 0.41 $W\text{cm}^{-2}$, respectively. Though the OCV values remain constant at 1.12 V on increase in temperature, the MPD values increase and reach 0.78, 1.78 and 2.1 $W\text{cm}^{-2}$ at 700, 750 and 800 °C, respectively, as given in Table 2. The NiO–YSZ functional layer increases the area of three phase boundary (TPB) at the electrolyte/fuel electrode interface and provides more reaction site for the fuel oxidation. Therefore, the higher values of power densities in button cell 2, compared to the button cell 1 at a fixed temperature, are mainly due to the better fuel utilization in button cell 2. Also, there is an improvement in the voltage drop with the increase in current density in button cell 2 in comparison to the button cell 1, which could again be attributed to the NiO–YSZ functional layer which improves the fuel electrode kinetics by providing additional reaction sites for the fuel oxidation. Fig. 5(b) shows the EIS complex plane plot of button cell 2 at different temperatures under open circuit conditions and the values of ASR obtained from the

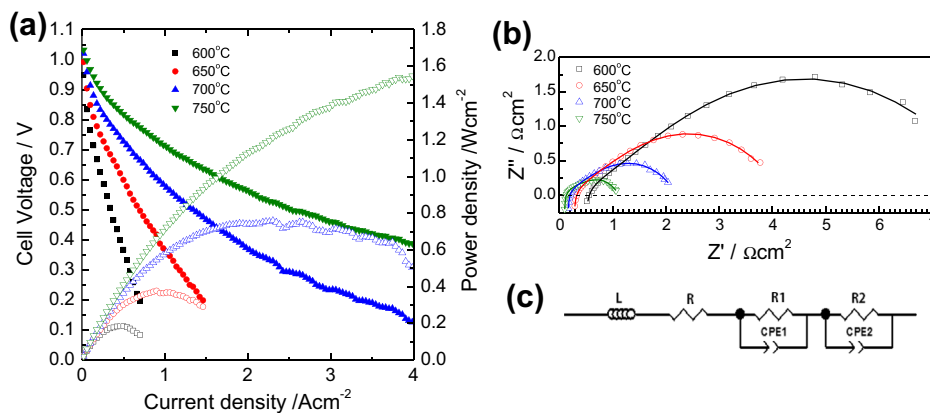


Fig. 4. (a) Performance of button cell 1 in SOFC mode at different temperatures; open symbol \Rightarrow power density, closed symbol \Rightarrow cell voltage, (b) EIS of button cell 1 at different temperatures under open circuit conditions, (c) equivalent circuit used for EIS data fitting.

Table 2
ASR, OCV and MPD of button cells in SOFC mode.

Temp./°C		Button cell 1	Button cell 2	Button cell 3
800	Total ASR _{EIS} /Ω cm ²	—	1.00	1.12
	ASR _{Electrode} /Ω cm ²	—	0.94	1.05
	ASR _{Ohmic} /Ω cm ²	—	0.06	0.07
	MPD/W cm ⁻²	—	2.10	1.68
	OCV/V	—	1.12	1.08
	Total ASR _{EIS} /Ω cm ²	1.14	1.22	1.55
750	ASR _{Electrode} /Ω cm ²	1.07	1.13	1.46
	ASR _{Ohmic} /Ω cm ²	0.07	0.09	0.09
	MPD/W cm ⁻²	1.54	1.78	0.99
	OCV/V	1.05	1.12	1.08
	Total ASR _{EIS} /Ω cm ²	2.21	2.58	3.08
	ASR _{Electrode} /Ω cm ²	2.07	2.43	2.98
700	ASR _{Ohmic} /Ω cm ²	0.14	0.15	0.10
	MPD/W cm ⁻²	0.74	0.78	0.54
	OCV/V	1.05	1.12	1.08
	Total ASR _{EIS} /Ω cm ²	4.23	4.71	—
	ASR _{Electrode} /Ω cm ²	4.01	4.46	—
	ASR _{Ohmic} /Ω cm ²	0.22	0.25	—
650	MPD/W cm ⁻²	0.38	0.41	—
	OCV/V	1.05	1.12	—
	Total ASR _{EIS} /Ω cm ²	8.32	—	—
	ASR _{Electrode} /Ω cm ²	7.96	—	—
	ASR _{Ohmic} /Ω cm ²	0.36	—	—
	MPD/W cm ⁻²	0.18	—	—
600	OCV/V	1.05	—	—
	Total ASR _{EIS} /Ω cm ²	—	—	—
	ASR _{Electrode} /Ω cm ²	—	—	—
	ASR _{Ohmic} /Ω cm ²	—	—	—
	MPD/W cm ⁻²	—	—	—
	OCV/V	—	—	—

equivalent circuit fitting are given in Table 2. Like the button cell 1, electrode ASR is the dominating factor in total ASR values, and the values of ohmic ASR and electrode ASR decrease with the increase in temperature. Furthermore, the ohmic ASR values of button cells 1 and 2 are comparable but the electrode ASR values of button cell 2 are slightly higher than that of button cell 1, which could be due to the fact that the combined thickness of NiO–YSZ/NiO–YSZ in button cell 2 is more than the thickness of the NiO–YSZ in button cell 1.

3.2.3. SOFC operation of button cell 3

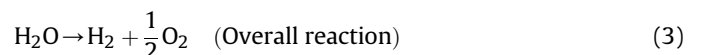
The button cell 3 is fabricated by replacing LSCF1982 oxygen electrode with a LSCF1982–GDC composite oxygen electrode. The performance of button cell 3 at different temperatures is shown in Fig. 6(a). At 700 °C, OCV and MPD are 1.08 V and 0.54 W cm⁻², respectively. Though the OCV values remain constant at 1.08 V on increase in temperature, the MPD values increase and reach 0.99 and 1.68 W cm⁻² at 750 and 800 °C, respectively, as given in Table 2. Fig. 6(b) shows the EIS of button cell 3 at different temperatures under OCV conditions and the values of ASR obtained from the equivalent circuit fitting are given in Table 2. Like the button cell 2, electrode ASR is the dominating factor in total ASR, and the values

of ohmic ASR and electrode ASR increases with the increase in temperature. However, for button cell 3, the values of power density and cell voltage, at a fixed current density and temperature, are lower than that for button cell 2. As given in Table 2, at a fixed temperature, the value of MPD in button cell 3 are lower than that in button cell 2. Also, the cell voltage drops rapidly with the increase in current density in button cell 3 in comparison to the button cell 2. Though ohmic ASR values of two cells are comparable, the electrode ASR values of button cell 3 are higher than that of button cell 2.

The button cells 2 and 3 use different oxygen electrode and the difference in their fuel cell performance could be attributed to the effectiveness of these electrodes in oxygen reduction at the TPB. In our previous studies [17,20], we have shown that LSCF1982 can be a good oxygen electrode material in SOFC, but based on the SOFC performance of the button cell 3, it appears that the LSCF1982–GDC composite has lower catalytic activity for oxygen reduction. This could be due to the lower oxygen ion conductivity and electronic conductivity of GDC compared to that of LSCF1982 [17,18,28,29]. Also, the difference in internal microstructures of two electrodes, leading to different utilization level of oxygen, could contribute to the difference in cell performance, especially at high current densities. However, the effect of poor conductivity of GDC is also visible with the increase in the values of electrode ASR on replacing LSCF1982 electrode with LSCF1982–GDC composite electrode (Table 2). Furthermore, there is a slight difference in the OCV values observed for the individual button cells 1–3, as given in Table 2. This minor variation could be due to the some issues related with the imperfections in glass sealing leading to some fuel leakage.

3.3. SOEC operation of button cells

The electrochemical reactions occurring in SOEC during steam electrolysis can be described by following equations [30]:



When steam is fed to the hydrogen electrode, it is reduced to hydrogen and oxide ion with the participation of two electrons from the external circuit. Oxide ions pass through the electrolyte to the oxygen electrode where they are oxidized to oxygen molecules,

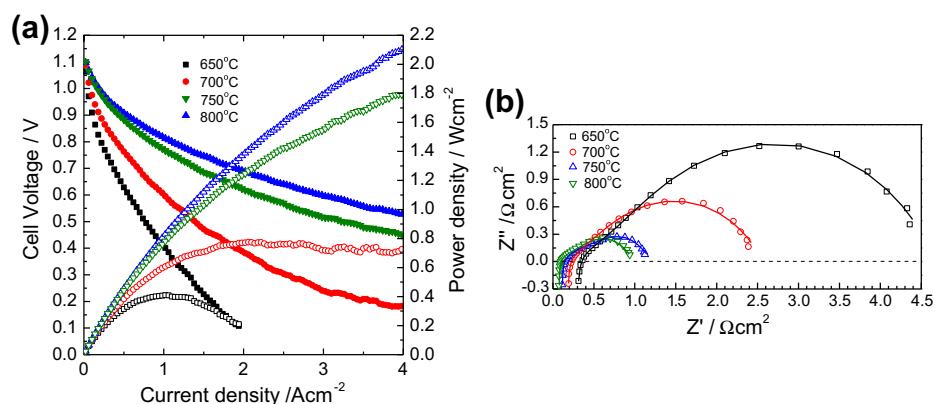


Fig. 5. (a) Performance of button cell 2 in SOFC mode at different temperatures; (b) EIS of button cell 2 at different temperatures under open circuit conditions.

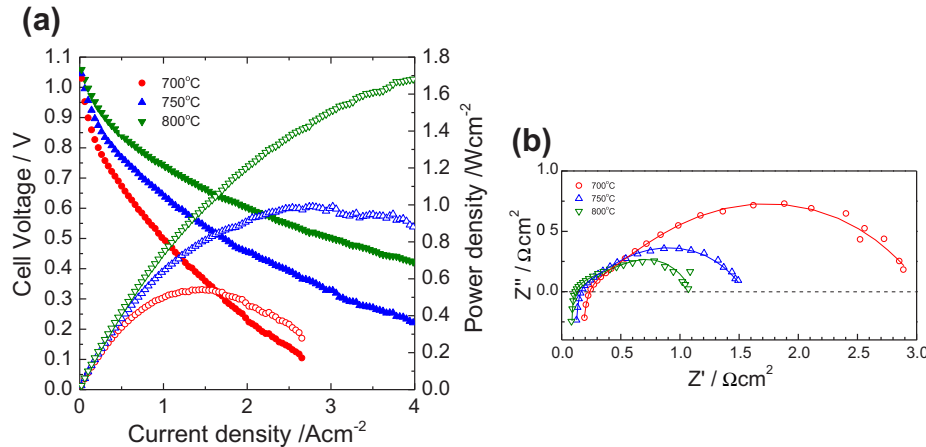


Fig. 6. (a) Performance of button cell 3 in SOFC mode at different temperatures; (b) EIS of button cell 3 at different temperatures under open circuit conditions.

releasing two electrons to the external circuit. For each mole of H₂O consumed, 1 mol of H₂ is generated and 2 mol of electrons are passed through the external circuit. Therefore, the hydrogen production rate from steam electrolysis in SOEC can be calculated directly from the measured current as follows [12]:

$$\Delta N_{H_2} = \frac{-I}{2F} \quad (4)$$

where ΔN_{H_2} is the molar rate of hydrogen production, I the electrical current and F the Faraday's constant. Alternatively, the performance of a solid oxide cell in SOEC mode can be defined in terms of cell voltage at a particular current density. Lower the cell voltage at a defined current density better is the SOEC performance[31].

3.3.1. SOEC operation of button cell 2

Button cell 2 shows best SOFC performance, as discussed in Section 3.2, and therefore, firstly button cell 2 was employed for SOEC operation. Fig. 7(a) shows EIS response of button cell 2 at OCV condition during SOEC operation at different temperatures. Like the SOFC mode, the impedance spectrum in SOEC mode consists of an elongated arc with a high frequency intercept on the real axis. The high frequency intercept is due to ohmic resistance mainly ascribed to the electrolyte whereas the elongated arc corresponds to the electrode phenomena. The appearance of an elongated arc indicates that more than one limiting phenomena are contributing to the processes at the electrode. The contributions of electrode ASR and ohmic ASR is calculated by fitting EIS data with an equivalent

circuit shown in Fig. 7(b) where L is the inductance and R is ohmic resistance; resistance $R1$ and constant phase element CPE1 corresponds to the charge transfer reaction at the electrode/electrolyte interface, and resistance $R2$ and constant phase element CPE2 corresponds to the adsorption/desorption and diffusion inside the porous electrode [27]. The ASR values obtained from equivalent circuit fitting are given in Table 3 and it can be seen that there is a large decrease in the total ASR value with the increase in temperature, and the decrease in electrode ASR value is the main contributing factor to this decrease. Since the electrolysis of water is a thermally activated process, the improvement in electrode ASR with the increase in temperature could be attributed to the consequent decrease in polarization of hydrogen electrode [16].

Fig. 8 shows the typical I – V curve for button cell 2 operating at 700, 750 and 800 °C. Negative values of current density indicate power consumption (the SOEC mode) while positive current densities indicate power generation (the SOFC mode). From the I – V curves, it can be seen that there is a smooth transition across the range of OCV from SOEC mode to SOFC mode, which indicates that the button cell 2 is reversible regarding the charge transfer reaction. It can be seen that at 700 °C the electrolysis voltage increases with the increase in current density. There is gradual change in the slope of the I – V curve on the application of a higher current density, leading to appearance of a plateau, as shown in Fig. 8. When temperature is increased to 750 °C and 800 °C, the slope of I – V curve decreases and lower electrolysis voltage is required for the hydrogen production. The voltage indicating the onset of the change in slope shifts to a higher current density with the increase in temperature. The improvement in the hydrogen production with the increase in temperature could be due to the reduction in energy

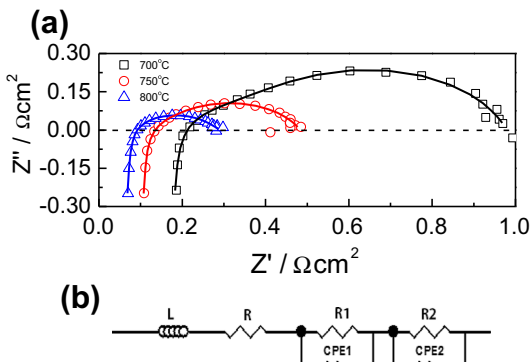


Table 3
ASR and OCV of button cells in SOEC mode.

Temp./°C		Button cell 1	Button cell 2	Button cell 3
800	Total ASR _{EIS} /Ω cm ²	—	0.293	0.487
	ASR _{Electrode} /Ω cm ²	—	0.244	0.432
	ASR _{Ohmic} /Ω cm ²	—	0.049	0.055
750	OCV/V	—	0.902	0.892
	Total ASR _{EIS} /Ω cm ²	0.709	0.483	0.885
	ASR _{Electrode} /Ω cm ²	0.617	0.386	0.814
700	ASR _{Ohmic} /Ω cm ²	0.092	0.097	0.071
	OCV/V	0.914	0.914	0.910
	Total ASR _{EIS} /Ω cm ²	—	0.979	1.625
0.923 V	ASR _{Electrode} /Ω cm ²	—	0.813	1.435
	ASR _{Ohmic} /Ω cm ²	—	0.166	0.190
0.923 V	OCV/V	—	0.930	0.926

Fig. 7. (a) EIS of button cell 2 at different temperatures under open circuit conditions, (b) Equivalent circuit used for EIS data fitting.

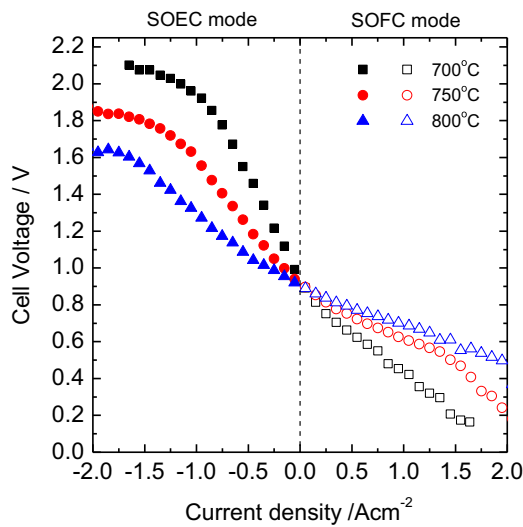


Fig. 8. I - V curves of button cell 2 at different temperatures.

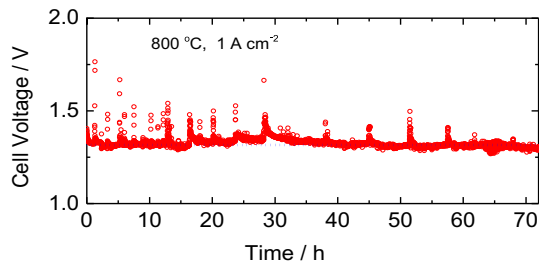


Fig. 9. Cell voltage of button cell 2 as a function of time, for an electrolysis current density of 1 A cm^{-2} , measured at 800 °C.

loss associated with the polarization of electrodes [16]. The EIS measurements in Fig. 7(a) have shown that electrode polarization is the major contributing factor in total ASR and, therefore, the improvements in the hydrogen production with the increase in temperature could be attributed to the improvement in electrode polarization.

The appearance of plateau at high current densities can be explained on the basis of oxide ion conduction across the electrolyte and oxygen evolution at the oxygen electrode, as they are some

of the limiting factors in SOEC operation of the solid oxide cell. At a particular temperature, when these limits, alone or together, are reached, the application of higher current density no longer translates into change in voltage. The voltage indicating the onset of the change in slope of I - V curve can be considered as the limit of SOEC operation of the cell. However, as above mentioned factors are thermally activated process, increase in temperature leads to increase in oxide ion conduction across the electrolyte and oxygen evolution at the oxygen electrode. Therefore, with the increase in temperature, the voltage indicating the onset of change in slope shifts to a higher current density. And, the SOEC operation at higher temperature not only leads to the better performance but also it shifts the operation limit to a higher current density.

3.3.1.1. Performance stability of button cell 2 in SOEC operation. In order to test the stability of performance of button cell 2 in SOEC mode, galvanostatic electrolysis operation was performed for 72 h at 800 °C. It is important to mention that an operation for 72 h may not give conclusive evidence about the long term stability of the button cell in SOEC operation, but such study arguably can provide some insight about its long term operation [16].

The galvanostatic electrolysis operation was performed for a hydrogen production rate corresponding to a current density of 1 A cm^{-2} . The cell voltage required to maintain the current density of 1 A cm^{-2} was plotted as a function of time, as shown in Fig. 9. It can be seen that during the operation for 72 h, cell voltage remains around 1.32 V. The intermittent fluctuations in the voltage are due to the change in steam flux while manual filling of water in syringe pump. Since a syringe with volume capacity of ~ 50 ml was used to deliver water in the syringe pump, it was needed to refill it after some time. The possible changes in steam flux during refilling are responsible for the intermittent fluctuations in cell voltage.

3.3.2. Effect of using $\text{NiO}-\text{YSZ}$ functional layer on the hydrogen electrode (comparison of SOEC operation of button cells 1 and 2)

During the SOEC operation of solid oxide cell, hydrogen electrode reaction (Eq. (1)) can be considered as the primary reaction, and is expected to be highly influenced by the nature (morphology and composition) of the hydrogen electrode, affecting the processes at the electrode and the resultant SOEC performance. Therefore, SOEC operation was also performed using the button cell 1 which, unlike the button cell 2, does not have a porous $\text{NiO}-\text{YSZ}$ functional layer. Fig. 10(a) shows the comparative I - V performance of button cells 1 and 2 at 750 °C. It is evident from the Fig. 10(a), for a fixed current density, the cell voltage of button cell 1 is higher than that

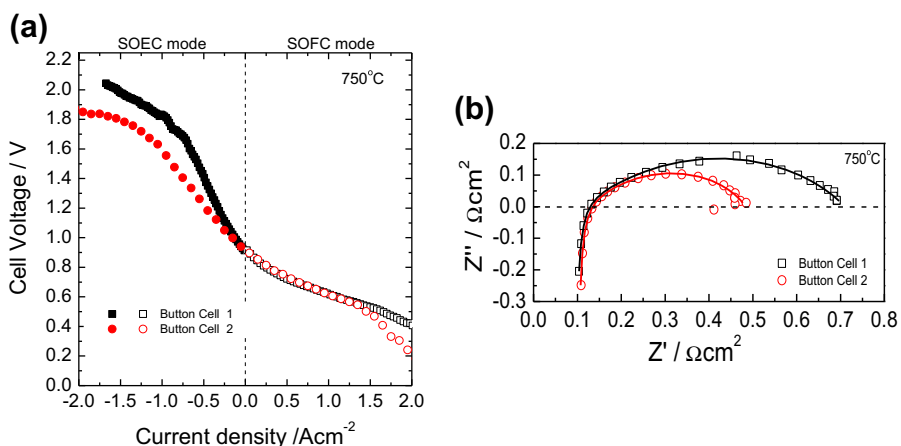


Fig. 10. (a) Comparative I - V performance of button cells 1 and 2 at 750 °C, (b) EIS measurement of button cell 1 and 2 at 750 °C under open circuit conditions.

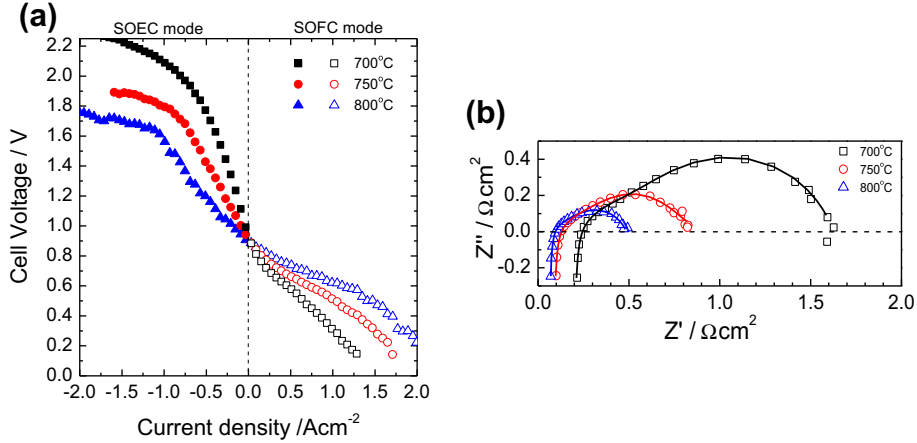


Fig. 11. (a) I – V curves of button cell 3 at different temperatures, (b) EIS of button cell 3 at different temperatures under open circuit conditions.

of the button cell 2, and the onset voltage indicating the limit of SOEC operation at high current density corresponds to a lower current density value in the button cell 1. Fig. 10(b) shows the EIS measurements of button cells 1 and 2 under OCV conditions at 750 °C. The position of high frequency intercept indicating the ohmic resistance remains constant for two cells but the size of the depressed semi-circular arc indicating the electrode response is greatly increased in the button cell 1. The ASR values calculated from the equivalent circuit fitting to the EIS data are given in Table 3. It is clear that though the ohmic ASR values of two cells are comparable, electrode ASR of the button cell 1 is nearly twice the electrode ASR of button cell 2. Since two cells differs only in terms of the presence/absence of porous NiO–YSZ functional layer, the improvements in the performance of button cell 2 can be attributed to the porous NiO–YSZ functional layer driven reduction in electrode polarization resistance. Like the operation in SOFC mode, the presence of porous functional layer reduces the electrode polarization resistance by increasing the area of TPB and improving the overall electrode kinetics at the hydrogen electrode.

3.3.3. SOEC operation of button cell 3

Fig. 11(a) shows the I – V curve for both SOFC and SOEC modes and Fig. 11(b) shows EIS of button cell 3 under open circuit conditions at 700, 750 and 800 °C. In general, the trends of variation in

different parameters are similar to those discussed in Section 3.3.1 for button cell 2. The electrolysis voltage increases with the increase in current density and on the application of a higher current density, there is gradual change in the slope of the I – V curve leading to appearance of a plateau. When the operating temperature is increased to 750 °C and 800 °C, the slope of I – V curve decreases and lower electrolysis voltage is required for the hydrogen production. Also, the voltage indicating the onset of the change in slope shifts to a higher current density with the increase in temperature. Similarly, the total ASR value decreases significantly with the increase in temperature and the decrease in electrode ASR is the major factor in this decrease (Table 3).

3.3.3.1. Effect of nature of oxygen electrode (comparison of SOEC operation of button cells 2 and 3). The performances of button cells 2 and 3 were compared in order to get insight into the effect of using different oxygen electrodes on the SOEC operation. Fig. 12(a) shows the I – V curve of button cells 2 and 3 at 800 °C and it can be seen that, at a fixed current density, the cell voltage of the button cell 3 is higher than that of button cell 2. Also, the onset voltage indicating the change in the slope of I – V curve is higher for the button cell 3. The impedance spectra shown in Fig. 12(b) and the ASR values given in Table 3 indicate that the button cell 2 shows lower polarization resistance than the button cell 3. Since the two

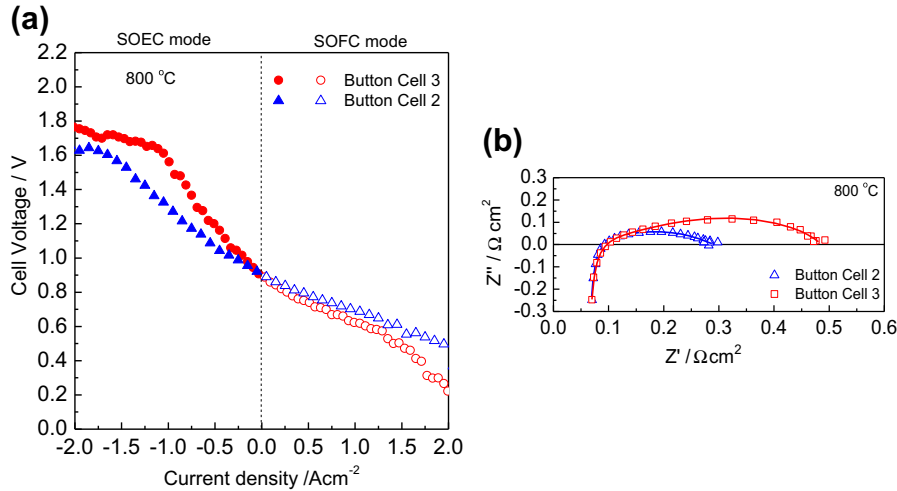


Fig. 12. (a) Comparative I – V performance of button cells 2 and 3 at 800 °C, (b) EIS measurement of button cell 2 and 3 at 800 °C under open circuit conditions.

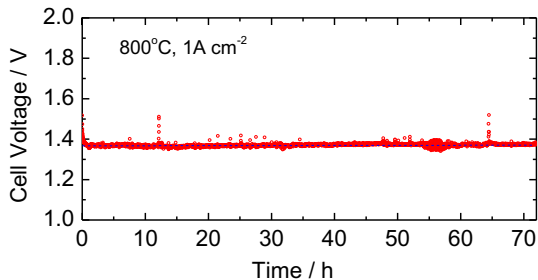


Fig. 13. Cell voltage of button cell 3 as a function of time, for an electrolysis current density of 1 A cm^{-2} , measured at 800°C .

cells differ in the nature of their oxygen electrode, the improvement in SOEC performance of button cell 2 could be attributed to the faster kinetics of oxygen electrode reaction (Eq. (2)) on LSCF1982 electrode than that on LSFC1982–GDC composite electrode.

3.3.3.2. Performance stability of button cell 3 in SOEC operation. In order to test the stability of performance of button cell 3 in SOEC mode, galvanostatic electrolysis operation was performed for 72 h at 800°C for a hydrogen production rate corresponding to a current density of 1 A cm^{-2} . The cell voltage required to maintain the current density of 1 A cm^{-2} was plotted as a function of time, as shown in Fig. 13. It can be seen that during the operation for 72 h, cell voltage remains around 1.37 V. The intermittent fluctuations in the voltage are due to the change in steam flux while manual filling of water in syringe pump. Therefore, though the button cell 3 operates at a higher cell voltage than that of button cell 2, like the button cell 2 it also shows a stable performance during the operation for 72 h.

3.4. Reversibility of solid oxide cells

3.4.1. Reversibility of button cell 2

In order to test the reversibility of the button cell 2, I – V test was performed on it after 3 days of continual galvanostatic operation discussed in Section 3.3.1.1. Fig. 14(a) shows the I – V curve of button cell 2 before galvanostatic test and after the galvanostatic test for 3 days at 800°C . It can be seen that I – V curves in SOEC mode are almost similar but there is larger drop in voltage in SOFC mode after the operation in galvanostatic mode. This indicates that though the

button cell 2 gives stable SOEC operation for an appreciably long duration, its reversibility is affected by such operation and leads to poor SOFC performance. The EIS curves, in Fig. 14(b), show that there is an increase in ohmic ASR of the cell after 3 days of galvanostatic operation. This could be due to the increase in contact resistance at the electrode/electrolyte interface, possibly because of the delamination [14] or because of grain growth inside the LSCF1982 oxygen electrode during the operation at 800°C [32,33]. However, effect of such delamination or grain growth is clearly visible only on SOFC operation, which can be explained on the basis of the nature of the primary reaction step during the SOFC/SOEC operations. In SOFC operation, reduction of oxygen ($\text{O}_2 + 2\text{e}^- \rightarrow \text{O}^{2-}$) at the oxygen electrode and subsequent transport of oxide ions across the electrolyte can be considered as the primary steps and they, alone or together, can be the rate determining. Therefore, delamination or grain growth on the oxygen electrode side would affect these steps and this, in turn, would lead to decrease in performance. On the other hand, in SOEC operation, the electrolysis of water at hydrogen electrode and subsequent transport of oxide ions across the electrolyte can be considered as the primary steps and, under given thermodynamic conditions, can be the rate determining. Therefore, delamination or grain growth on the oxygen electrode side shows minimal effect on the SOEC operation, even after 3 days, though the possibility of these effects becoming significant, on SOEC operation for longer duration, cannot be denied.

In order to further ascertain the reversibility of button cell 2, successive SOFC/SOEC operations were run at 800°C in such a manner as mentioned below:

1st SOFC operation \rightarrow SOEC operation (galvanostatic for 1 day) \rightarrow 2nd SOFC operation.

During the SOEC operation following the 1st SOFC, button cell shows stable performance, and for a current density of 1 A cm^{-2} cell voltage remains around 1.32 V (data not shown), which is similar to that observed in Section 3.3.1.1. However, a significant reduction in the SOFC performance is observed for 2nd operation in comparison to 1st operation, as shown in Fig. 15(a). Though the value of OCV is comparable ($\sim 1.1 \text{ V}$), in 2nd SOFC operation, the maximum power density is smaller and the decrease in cell voltage at higher current densities is larger. Fig. 15(b) shows the corresponding EIS measurements in OCV condition in SOFC mode. Though the position of high frequency intercept, which indicates ohmic ASR, is constant, the position of low frequency intercept slightly shifts to right, indicating an increase in electrode ASR. Based on EIS measurements, it appears that grain growth inside the oxygen electrode

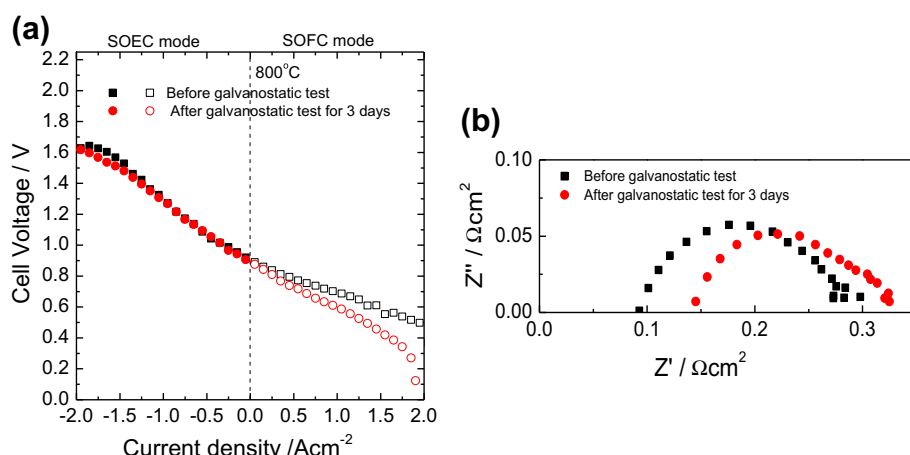


Fig. 14. (a) I – V curves of button cell 2 for successive measurements at 800°C , (b) EIS of button cell 2 for successive measurements at 800°C under open circuit conditions.

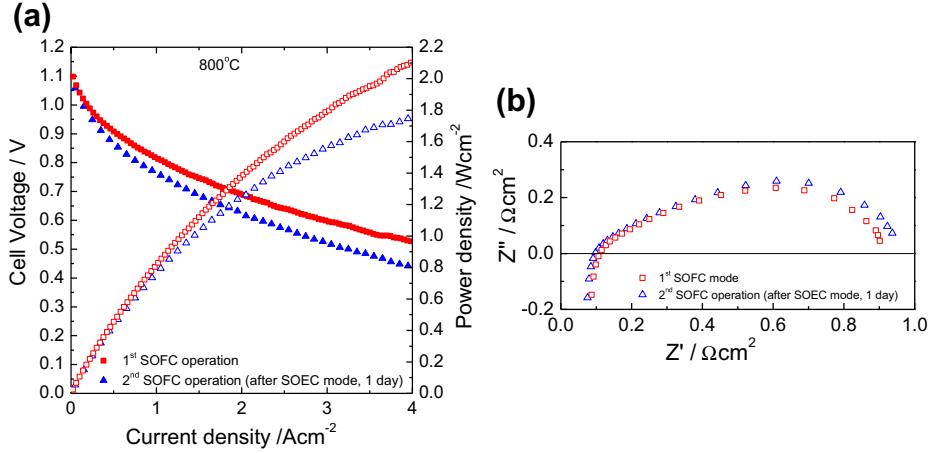


Fig. 15. (a) Performance of button cell 2 in SOFC mode at 800 °C; (b) EIS of button cell 2 in OCV conditions during SOFC operation.

could be the reason of decrease in power density in 2nd SOFC operation, as grain growth inside the electrode may affect the flow of gases inside the porous electrode.

3.4.2. Reversibility of button cell 3

The reversibility of the button cell 3 was tested in the same way as discussed for the button cell 2 in Section 3.4.1. Fig. 16(a) shows the *I*–*V* curve of button cell 3 for successive measurements- before the galvanostatic test and after the galvanostatic test for 3 days. It can be seen that, like in the case of button cell 2, *I*–*V* curves in SOEC mode are almost similar but there is larger drop in voltage at high current density in SOFC mode after the operation in galvanostatic mode. This indicates that though the button cell 3 gives stable SOEC operation for an appreciably long duration, its reversibility is affected by such operation and leads to poor SOFC performance, like in the case of button cell 2. The EIS curves in Fig. 16(b) show that there is an increase in ohmic ASR and electrode ASR of the cell after 3 days of galvanostatic operation. The delamination or grain growth on the oxygen electrode side could be the reason for the increase in ARS values which affect differentially in SOEC/SOFC mode, as previously discussed for button cell 2 in Section 3.4.1.

In order to further ascertain the reversibility of button cell 3, successive SOFC/SOEC operations were run at 800 °C in such a manner as mentioned below:

1st SOFC operation → SOEC operation (galvanostatic for 3 days) → 2nd SOFC operation.

During the SOEC operation following the 1st SOFC, button cell shows a stable performance and for a current density of 1 A cm⁻² cell voltage remains ~1.37 V (data not shown), which is similar to the observation in Section 3.3.3.2. On comparing the SOFC performance during 1st and 2nd operations, however, a significant reduction in the SOFC performance is observed for 2nd operation, as shown in Fig. 17(a). In 2nd SOFC operation, the MPD decreases significantly and there is a sharp drop in power density and cell voltage at higher current densities, indicating a significant increase in losses due to the concentration polarization. Fig. 17(b) shows the corresponding EIS measurements in OCV condition in SOFC mode, which indicates that though ohmic ASR is constant; the value of electrode ASR is higher for 2nd operation. As discussed earlier in Section 3.4.1, grain growth inside the oxygen electrode could be the reason of ohmic ASR in 2nd SOFC operation.

The increase in flow rate of gases can improve the performance of fuel cell by improving electrode polarization and by increasing the availability of reactants at the TPB, due to the increase in convective flow inside the porous electrode [34]. During the 2nd SOFC operation of the button cell 3, when the flow rate of H₂ on hydrogen electrode is increased from 100 sscm to 150 sscm, however, there is no change in SOFC performance, but when the flow

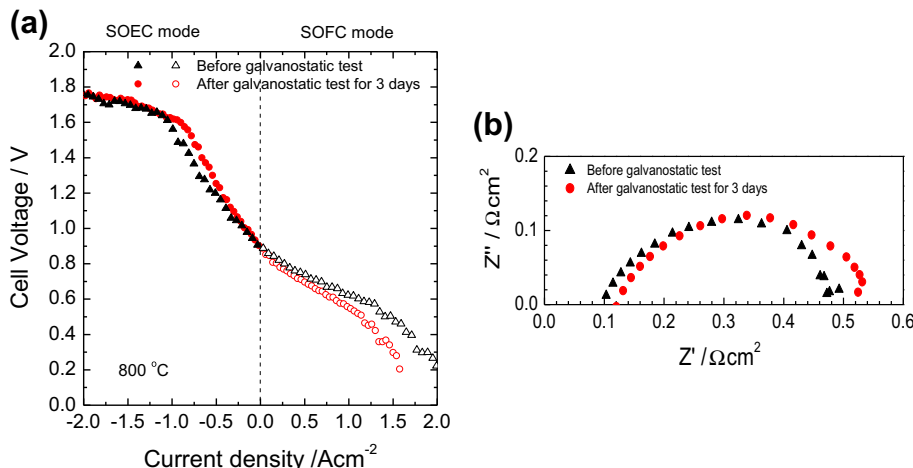


Fig. 16. (a) *I*–*V* curves of button cell 3 for successive measurements at 800 °C, (b) EIS of button cell 3 for successive measurements at 800 °C under open circuit conditions.

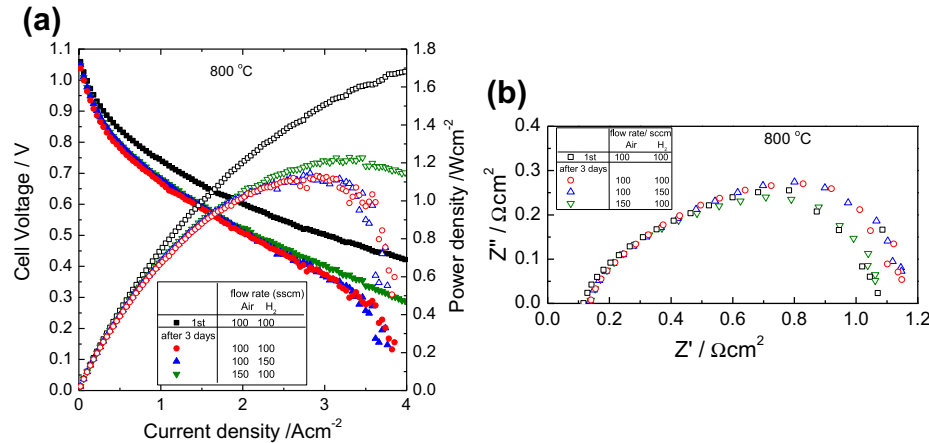


Fig. 17. (a) Performance of button cell 3 in SOFC mode at 800 °C, (b) EIS of button cell 2 in OCV conditions during SOFC operation.

rate of O₂ on the oxygen electrode is increased from 100 sccm to 150 sccm there is a significant improvement in power density and cell voltage at higher current density, as shown in Fig. 17(a), indicating an improvement in losses due to the concentration polarization. The EIS data corresponding to flow rate change, as given in Fig. 17(b), shows that the decrease in electrode polarization is observed only on increasing the flow rate at the oxygen electrode side. This observation further indicates that it is the stability of LSCF1982–GDC oxygen electrode which affects the reversibility of button cell 3.

3.4.3. Comparison of reversibility of button cells 2 and 3

The use of composite electrodes, having electrolyte as one of its constituents, helps improving the stability of cell by enhancing the compatibility of electrolyte and electrode materials at their interface. Therefore, using LSCF1982–GDC composite oxygen electrode, better durability of the button cell 3 is expected. Comparing the EIS data of button cell 2 (Fig. 14(b)) and button cell 3 (Fig. 16(b)), it is clear that the shift in the position of high frequency intercept corresponding to ohmic ASR is more in button cell 2 than that in button cell 3. Such increase in ohmic ASR may be due to the loss in interfacial contact between the electrolyte and electrode [32,33], probably because of the differential thermal expansion of two components. In the present study, thermal expansion coefficient of LSCF1982 is higher than GDC [17,35]. Therefore, long term operation at high temperature may lead to loss of contact at GDC barrier

layer/oxygen electrode interface in button cell 2. In LSCF1982–GDC composite, the use of GDC increases the compatibility between GDC barrier layer and LSCF1982–GDC composite oxygen electrode, and therefore, minimizes the loss of contact at GDC barrier layer/oxygen electrode interface in button cell 3 and enhances its durability. The better durability of LSCF1982–GDC composite cathode is also visible on comparing the *I*–*V* curves of successive SOFC → SOEC → SOFC operations, as shown in Fig. 18. It can be seen, in button cell 2 the difference in two MPD values is larger than that in button cell 3.

3.5. Stability of microstructure of button cell on reversible SOFC/SOEC operation

The scanning electron microscopy is used to study the microstructure of the button cell assembly after successive SOFC/SOEC operations. Fig. 19 shows the SEM micrographs of the cross section of button cells after one successive SOFC/SOEC operations. In every button cell, the GDC barrier layer is <2 μm thick and the cross section of button cell has no observable internal cracks, either between oxygen electrode and barrier layer or barrier layer and electrolyte, which indicated that the dense GDC barrier layer has been compatible with LSCF1982 or LSCF1982–GDC oxygen electrode layer and YSZ electrolyte layer, and it successfully prevents the reaction between LSCF1982 and YSZ electrolyte during the RSOC measurements at temperatures ≤ 1000 °C. The delamination

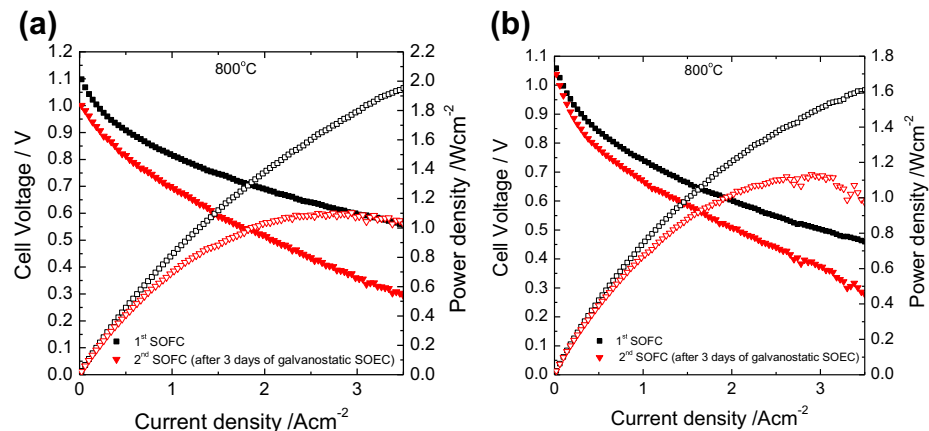


Fig. 18. Performance of (a) button cell 2 and (b) button cell 3 at 800 °C on successive operation in SOFC → SOEC (for 3 days) → SOFC modes.

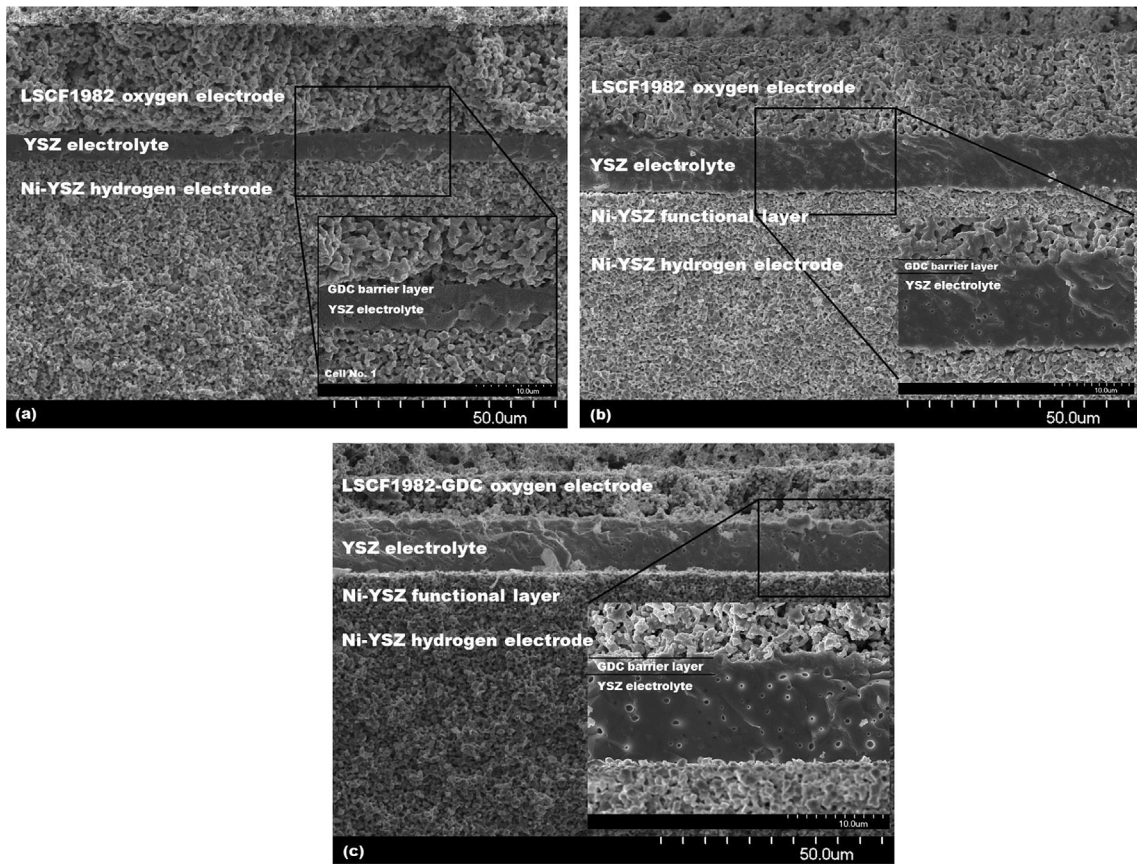


Fig. 19. SEM images of cross-section of the button cells 1–3 after the ROSC operation.

of the oxygen electrode is not visible from SEM images, but based on the results of cell performance and EIS measurements, the possibility of interfacial degradation cannot be denied. However, Fig. 19(b) shows some delamination between YSZ electrolyte and Ni–YSZ functional layer. Though it is difficult to clearly indicate the reason for this, but based on the common observation that the SOEC operation normally causes the delamination between oxygen electrode and electrolyte, the observed delamination in Fig. 19(b) could occur during the SEM sample preparation.

4. Conclusion

In this work, LSCF1982 and LSCF1982–GDC composite oxygen electrodes with GDC barrier layer are tested in YSZ electrolyte-based RSOCs at different temperatures ($600 \leq ^\circ\text{C} \leq 800$). Three button cell assemblies (Button cell 1: NiO–YSZ|YSZ/GDC|LSCF1982; Button cell 2: NiO–YSZ/NiO–YSZ|YSZ/GDC|LSCF1982; and Button cell 3: NiO–YSZ/NiO–YSZ|YSZ/GDC|LSCF1982–GDC) are fabricated, and the effect of using NiO–YSZ functional layer on hydrogen electrode side on the performance in SOFC mode as well as in SOEC mode is studied, which indicates improvements in SOFC/SOEC performance. The effect of nature of oxygen electrode on the SOFC/SOEC performance is studied, which indicates better SOFC/SOEC performance by LSCF1982 oxygen electrode than with LSCF1982–GDC composite oxygen electrode. In SOFC mode, button cell 1 shows maximum power density of 1.54 W cm^{-2} at 750°C . The use of NiO–YSZ functional layer on the hydrogen electrode helps improving the cell performance by improving the area of TPB, but the replacement of LSCF1982 oxygen electrode with a LSCF1982–GDC composite oxygen electrode leads to decrease in cell

performance due to the lower oxide-ion and electron conductivity of LSCF1982–GDC composite in comparison to the LSCF1982. In SOFC mode, button cells 2 and 3 respectively show maximum power density of 2.1 W cm^{-2} and 1.68 W cm^{-2} at 800°C . In SOEC mode, button cell 2 shows the best performance with cell voltage reaching to 1.6 V for current density of 1.65 A cm^{-2} at 800°C . Stability of the button cells is studied by 72 h galvanostatic SOEC operation as well as by reversible SOFC/SOEC operations. *I*–*V* tests and EIS measurements indicates that the button cells show stable operation in SOEC mode. But successive SOFC → SOEC → SOFC operations indicate that the cells are not completely reversible. The possible reason for irreversibility is found to be related with the oxygen electrode, and the button cell with LSCF1982–GDC composite oxygen electrode is more stable than the button cell with LSCF1982 oxygen electrode.

Acknowledgments

This work was supported by Priority Research Centers Program through the National Research Foundation of Korea (NRF), funded by the Ministry of Education, Science and Technology (2009-0094055).

References

- [1] O.A. Marina, L.R. Pederson, M.C. Williams, G.W. Coffey, K.D. Meinhardt, C.D. Nguyen, E.C. Thomson, *J. Electrochem. Soc.* 154 (2007) B452–B459.
- [2] M. Mogensen, S.H. Jensen, A. Hauch, J. Chorkendorff, T. Jacobsen, in: *Advances in Solid Oxide Fuel Cells III: Ceramic and Engineering Science Proceeding*, 28, 2008, pp. 91–101, 4.
- [3] J. Ren, S.R. Gamble, A.J. Roscoe, J.T.S. Irvine, G. Burt, *Fuel Cells* 12 (2012) 773–786.

- [4] N.Q. Minh, ECS Trans. 35 (2011) 2897–2904.
- [5] S.H. Jensen, P.H. Larsen, M. Mogensen, Int. J. Hydrogen Energy 32 (2007) 3253–3257.
- [6] M. Ni, M.K.H. Leung, D.Y.C. Leung, Int. J. Hydrogen Energy 33 (2008) 2337–2354.
- [7] C.M. Stoots, J.E. O'Brien, K.G. Condie, J.J. Hartvigsen, Int. J. Hydrogen Energy 35 (2010) 4861–4870.
- [8] P. Kim-Lohsoontorn, N. Laosiripojana, J. Bae, Curr. Appl. Phys. 11 (2011) S223–S228.
- [9] P. Kim-Lohsoontorn, D.J.L. Brett, N. Laosiripojana, Y.M. Kim, J.M. Bae, Int. J. Hydrogen Energy 35 (2010) 3958–3966.
- [10] M.A. Laguna-Bercero, J.A. Kilner, S.J. Skinner, Chem. Mater. 22 (2010) 1134–1141.
- [11] W. Wang, Y. Huang, S. Jung, J.M. Vohs, R.J. Gorte, J. Electrochem. Soc. 153 (2006) A2066–A2070.
- [12] J.E. O'Brien, C.M. Stoots, J.S. Herring, P.A. Lessing, J.J. Hartvigsen, S. Elangovan, J. Fuel Cell Sci. Technol. 2 (2005) 156–163.
- [13] K. Eguchi, T. Hatagishi, H. Arai, Solid State Ionics 86–88 (1996) 1245–1249.
- [14] A.V. Virkar, Int. J. Hydrogen Energy 35 (2010) 9527–9543.
- [15] B. Yu, W.Q. Zhang, J.M. Xu, Int. J. Hydrogen Energy 33 (2008) 6873–6877.
- [16] W. Zhang, B. Yu, J. Xu, Int. J. Hydrogen Energy 37 (2012) 837–842.
- [17] M.B. Choi, S.Y. Jeon, J.Y. Park, H.S. Yang, S.J. Song, Solid State Ionics 192 (2011) 269–274.
- [18] M.B. Choi, D.K. Lim, E.D. Wachsman, S.J. Song, Solid State Ionics 221 (2012) 22–27.
- [19] S.Y. Jeon, M.B. Choi, J.Y. Park, S.J. Song, J. Ceram. Process. Res. 12 (2011) 26–29.
- [20] M.B. Choi, K.T. Lee, H.S. Yoon, S.Y. Jeon, E.D. Wachsman, S.J. Song, J. Power Sources 220 (2012) 377–382.
- [21] A.J. Jacobson, Chem. Mater. 22 (2010) 660–674.
- [22] R.N. Blumenthal, F.S. Brugner, J.E. Garnier, J. Electrochem. Soc. 120 (1973) 1230–1237.
- [23] T. Suzuki, Z. Hasan, Y. Funahashi, T. Yamaguchi, Y. Fujishiro, M. Awano, Science 325 (2009) 852–855.
- [24] A. Momma, T. Kato, Y. Kaga, S. Nagata, J. Ceram. Soc. Jpn. 105 (1997) 369–373.
- [25] A. Hauch, S.H. Jensen, M. Mogensen, Roskilde, Denmark, in: S. Linderoth, A. Smith, N. Bonanos, A. Hagen, L. Mikkelsen, K. Kammer, D. Lybye, P.V. Hendriksen, F.W. Poulsen, M. Mogensen, W.G. Wang (Eds.), Proceedings of the 26th Risø International Symposium on Materials Science: Solid State Electrochemistry, Roskilde, Denmark, 2005, p. 203.
- [26] K.T. Lee, D.W. Jung, M.A. Camaratta, H.S. Yoon, J.S. Ahn, E.D. Wachsman, J. Power Sources 205 (2012) 122–128.
- [27] C. Arrive, T. Delahaye, O. Joubert, G. Gauthier, J. Power Sources 223 (2013) 341–348.
- [28] S.H. Park, H.I. Yoo, Phys. Chem. Chem. Phys. 11 (2009) 391–401.
- [29] T.S. Zhang, P. Hing, H.T. Huang, J. Kilner, Solid State Ionics 148 (2002) 567–573.
- [30] A. Brisse, J. Schefold, M. Zahid, Int. J. Hydrogen Energy 33 (2008) 5375–5382.
- [31] S.H. Jensen, X. Sun, S.D. Ebbesen, R. Knibbe, M. Mogensen, Int. J. Hydrogen Energy 35 (2010) 9544–9549.
- [32] Y.L. Liu, K. Thyden, M. Chen, A. Hagen, Solid State Ionics 206 (2012) 97–103.
- [33] V. Dusastre, J.A. Kilner, Solid State Ionics 126 (1999) 163–174.
- [34] K.C. Lee, M.B. Choi, D.K. Lim, B. Singh, S.J. Song, J. Power Sources 232 (2013) 224–233.
- [35] E.V. Tsipis, V.V. Kharton, J. Solid State Electrochem 12 (2008) 1039–1060.